Hindawi
Advances in Civil Engineering
Volume 2022, Article ID 5352330, 14 pages
https://doi.org/10.1155/2022/5352330

Research Article

Shear Strengthening of RC Deep Beams with Symmetrically or Asymmetrically Positioned Square Openings Using CFRP Composites and Steel Protective Frames

Hamid Karimizadeh,[1] **Abolfazl Arabzadeh**,[2] **Mohammad Reza Eftekhar**,[3] **and Asghar Amani Dashlejeh**[4]

[1]*Faculty of Civil and Environmental Engineering, Tarbiat Modares University, Tehran, Iran*
[2]*Faculty of Civil and Environmental Engineering, Tarbiat Modares University, Tehran, Iran*
[3]*Faculty of Civil Engineering, Isfahan University of Technology, Isfahan, Iran*
[4]*Faculty of Engineering, University of Mohaghegh Ardabili, Ardabil, Iran*

Correspondence should be addressed to Hamid Karimizadeh; h.karimizadeh@modares.ac.ir

Received 13 April 2022; Revised 11 July 2022; Accepted 21 August 2022; Published 19 September 2022

Academic Editor: Tan-Trung Bui

In most cases, openings are made in the Web of deep beams for installations to pass through. These members require to be strengthened since the openings reduce load-bearing capacity. This study utilizes carbon fiber-reinforced polymer (CFRP) composites and steel protective frames (SPF) as strengthening configurations in reinforced concrete (RC) deep beams to improve the strength lost due to the square openings. To this end, eleven specimens with $10 \times 50 \times 120$ cm in size were subjected to the three-point monotonic loading. In each beam, one or two square openings of 18 cm in each side are positioned either symmetrically or asymmetrically along the beam before it is strengthened with CFRP composites or SPFs. The strengthening composites were installed using externally bonded reinforcement (EBR) or externally bonded reinforcement on grooves (EBROG) techniques in two wrapped or inclined configurations. The obtained results indicate that specimens retrofitted by the SPF exhibited a superior performance as their loading capacity and energy absorption were enhanced by 115% and 337% in comparison with the reference beam, respectively, while these values for the specimens retrofitted by the EBROG technique were 58% and 182%, respectively, and 42% and 105% for those strengthened with the EBR technique.

1. Introduction

The large depth of reinforced concrete (RC) deep beams creates problems for housing electrical and mechanical installation. However, consideration of the openings in the Web of the beam solves this problem, and installations can be passed through the beam. The presence of such openings leads to discontinuities in load transfer paths and causes a considerable reduction of the load-bearing capacity of the beam. Provision of these openings in the design stage before beam construction allows designers to create structural properties that will successfully prevent such declines in strength; however, the need for such openings emerges in most cases after the beam has been constructed when its strengthening is found inevitable [1–6].

One solution proposed to compensate for the low strength due to openings in deep beams is the use of fiber-reinforced polymer (FRP) composite sheets [7–10]. Depending on their failure mode, beams may be strengthened against either flexural or shear failure. Flexural strengthening is accomplished through the externally bonded reinforcement (EBR) [11–13], near surface mounted (NSM) [12, 14–17], externally bonded reinforcement on grooves (EBROG), or externally bonded reinforcement in grooves (EBRIG) [18–20] techniques whereby FRP sheets are installed on lower beam parts with positive bending

moments and the upper beam parts with negative bending moments. Since ultimate failure in deep beams occurs with shear cracks in their Web, the composite retrofits are installed on the beam Web.

In recent years, some retrofitting techniques were presented by researchers. El-Maaddawy and Sherif [7] subjected their CFRP-strengthened deep beams with square openings created in different positions to the four-point test to observe shear strength enhancements of 35% to 75% as a result of the FRP retrofits used. Moreover, the authors reported that the closer the openings were to the beam top, the stronger the beam would become against shear loadings; this was attributed to the increased confinement effect in the bottom region. Finally, the authors reported that the FRP-strengthened specimens with openings in the middle of their Webs exhibited higher stiffness levels than did those with openings on their top or bottom sides.

Mostofinejad and Mahmoudabadi [21] were the first to employ the grooving method to prevent FRP debonding. These authors compared three techniques of installing CFRP retrofits on normal beams: one with no surface preparation, one with surface preparation, and one with (longitudinal, inclined, or diagonal) grooves of different depths. The results showed the considerable effect of the grooving method to prevent FRP debonding. Mostofinejad and Hajrasouliha [22] carried out a more in-depth investigation of the parameters involved in the grooving method. The authors found that a groove depth of 10 mm and a groove width of 8 mm were optimized dimensions for preventing early debonding of their retrofits.

El-Maaddawy and El-Ariss [10] investigated the effects of FRP strengthening on existing deep beams with openings in their Webs to find that failure in such strengthened beams started with the debonding and/or rupture of the FRP sheets at the corners of the openings due to stress concentration in these regions. Moreover, the authors observed splitting cracks at the top surface of the beam parallel to the compression reinforcement appearing right before or after the failure in highly strengthened beams. They attributed this to the transitional tensile stresses formed on the top surface as a result of the high compression stress in the compression reinforcement. The low thickness and compression strength of the beam combined with its high shear strength due to the high number of FRP retrofits used caused the cracks to propagate at the top side of the beam, while the strengthening sheets at the bottom and around the openings in the nonstrengthened beams confined the longitudinal reinforcement and, thus, removed the longitudinal cracks created at the bottom.

Arabzadeh and Karimizadeh [8] used CFRP composites in the three wrapped, vertical, and inclined configurations installed through the EBR and EBROG techniques for shear strengthening of deep beams with symmetrically or asymmetrically positioned circular openings. The results of their experiment showed the superior effects of the EBROG technique on increasing load-bearing capacity and ductility in their specimens. The authors also found that the inclined configuration of FRP retrofits led to the highest increases in both load-bearing capacity and ductility.

Based on the above reports, the present study was designed and implemented to develop a proper method for shear strengthening of RC deep beams to compensate for the lost strength due to the openings created in the beam web. For this purpose, the two methods of strengthening with CFRP composites and steel protective frames (SPF) are employed. In the first method, a detailed description of which was presented in the Introduction, the two EBR and EBROG techniques are used to either wrap CFRP retrofits around the beam or to install them at an inclined angle of 45 degrees. An alternative to these two configurations would be the vertical configuration, which is skipped in the present experiment since its inefficiency has already been discovered in a previous experiment by the present authors [8]. The openings made in the beam specimens are square-shaped and symmetrically or asymmetrically positioned on the beam web such that they largely intersect the stress transfer path in the struts.

The second method used involves the use of an SPF that surrounds the opening to serve as a truss compression member transferring loads to support points. Moreover, the SPF is made such that it accommodates an opening in it exactly matching the location of the beam opening, thereby allowing the opening to serve its expected function of passing installations. Thus, the study strives to determine the effects of the following parameters on shear strengthening of deep beams: (1) FRP retrofits and SPFs, (2) groove specifications, (3) loading plate thickness, and (4) positional symmetrical of openings.

2. Test Specifications

2.1. Preparation of Specimens. For this study, 11 deep RC beams (each 120 cm in length, 50 cm in height, and 10 cm in width with net spans of 100 cm and identical strengths) were uniformly constructed and subjected to the three-point monotonic bending test. The specimens were different in their retrofitting arrangements and openings position. For each specimen, three steel plates of identical thickness were used at the loading and support points to prevent plate bearing failure. To determine the effects of plate thickness at loading and support points, two control specimens were also constructed, one with a plate 15 mm thickness and the other similar to the experimental ones with a plate 30 mm thickness. Stress concentration at support and loading points in the beams was prevented by welding two U-shaped Φ12 steel bars to the steel loading plates. All the plates were installed in the mold before concrete pouring. Reinforcement used in the beams complied with ACI 318 [23] (Figure 1(a)). Table 1 reports the mechanical properties of the steel rebars used in the test.

The concrete utilized had a characteristic compressive strength of 40 MPa, which was achieved by using a concrete mix design based on Table 1. The compressive strength of each beam specimen was determined by testing three standard cylindrical samples ($300 * 150$ mm) of each specimen. Similar to the experimental specimens, the cylindrical samples were removed from their molds one day after concrete placement and subsequently cured for 27 days in a water pool at 25 to 28°C.

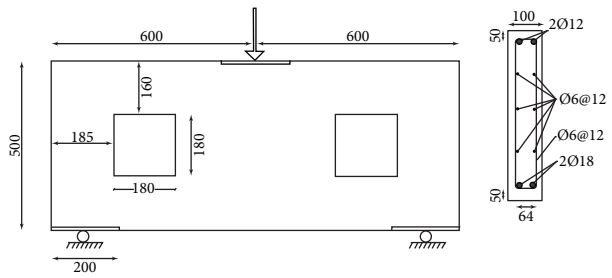

Figure 1: Reinforcement details (dimensions in mm).

Table 1: Material properties.

Steel (mm bars)	Diameter (mm)		Yield strength (MPa)		Ultimate tensile strength (MPa)
6	6		300		495
12	12		398		728
18	18		472		667
Concrete	Water (kg/m^3)	Cement (kg/m^3)	Fine aggregate (kg/m^3)	Coarse aggregate (kg/m^3)	Standard deviation (MPa)
f'_c = 40Mpa	181	467	1175	759	4.7
Resin	Tensile strength (MPa)		Elastic modulus (GPa)		Ultimate tensile strain (%)
Sikadur-330	30		4.5		0.9
Fiber	Tensile strength (MPa)	Elastic modulus (GPa)	Ultimate tensile strain (%)		Thickness (mm)
Sika wrap-200 C	3900	230	1.5		0.9

The square openings created were 18 cm on each side and distributed either symmetrically or asymmetrically along the beam so that they would cut across a large part of each stress path. The symmetrically positioned openings are shown in Figure 1(b), and only one of the asymmetrical openings remained in its original position.

2.2. Strengthening Methods. The specimens were strengthened using either CFRP retrofits with a suitable resin (specifications reported in Table 1) or steel protective frames of steel St37 as shown in Figure 2. As already mentioned, 11 deep beams of identical characteristics were constructed with different strengthening methods, retrofitting configuration, and opening symmetry. Furthermore, four specimens without any retrofitting were used as reference specimens. The control specimens with no openings in them were labeled *C*1 and *C*2; these differed only in the thickness of their loading and support plates such that the plate thickness in *C*1 was 30 mm while that in *C*2 was 15 mm. The remaining two specimens (i.e., the reference ones) had asymmetrically (*E*) or symmetrically (*S*) positioned openings in them (Figures 3(a) and 3(b)). The designations used for the other specimens include an initial part representing opening positional symmetricity followed by the strengthening technique (EBR or EBROG) used, and the letters *W* and *F* standing for wrapping and SPF, respectively. Figure 3 presents the different strengthening methods and opening positions in the specimens.

While the EBR technique involves installing the CFRP sheets directly on the concrete surface via the wet layup method, the EBROG technique begins with an initial step of making grooves about 10 mm in both width and depth in the concrete where the FRP strips are installed. This step is followed by filling the grooves with adequate resin. Figure 2 shows schematically the procedures for FRP installation in both EBR and EBROG techniques. All the retrofits were 5 cm in width; however, those used in specimen strengthened with FRP wraps that extended to the openings were 8 cm in width. In case the FRP sheets were discontinued, the retrofits would be extended to the concrete surface and opening edges to cover lengths of 5 cm of the upper and lower surfaces to provide complete confinement and to prevent early debonding. In the specimens strengthened with SPFs, steel frames of a height equal to the specimen's width (with openings prefabricated in them to serve as expected beam openings) were initially constructed and fixed in place within the mold before concrete casting such that the frame would be embedded in concrete (Figures 2(d), 2(e), 3(g), and 3(h)). The SPFs in this experiment were used to determine whether load transfer would occur on one or both sides of the frame. Hence, a frame thickness of 25 mm was selected at its most critical zone (i.e., the arch) so that it would not fail under loading. Additionally, the inside of the frame shown in Figure 2 that is circular plays no role in the load transfer process. This property can be replicated in square openings so that the frame looks square-shaped from the inside but

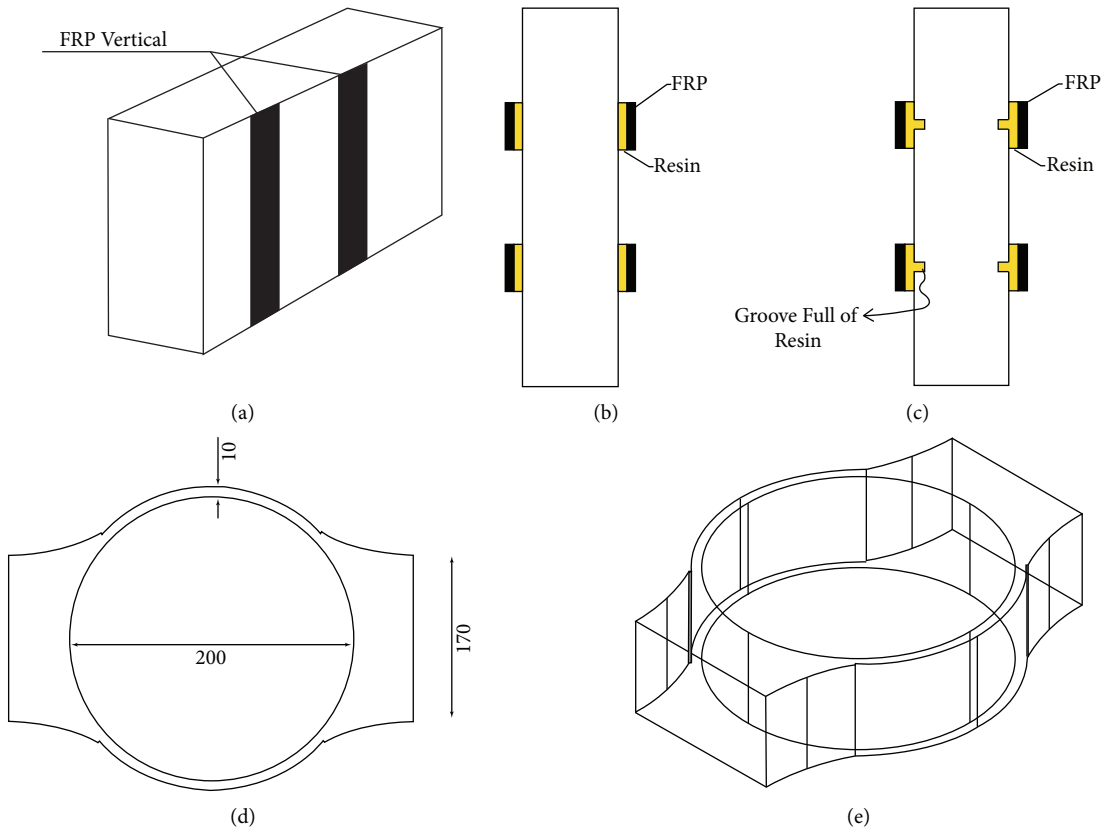

Figure 2: Schematic representation of FRP installation via the EBR and EBROG techniques as well as that of steel frames: (a) vertical strengthening of a beam via the EBR or EBROG technique; (b) EBR; (c) EBROG; (d) 2D plane of a steel frame (dimensions in mm); and (e) 3D plane of a steel frame. *Note: the resin, fiber, and groove dimensions are far larger than their real size.

circular from the outside. The external circular shape was adopted to avoid extreme stress concentration in the corners of square frames.

2.3. Test Method. A steel frame as shown in Figure 4(a) was used to implement the three-point flexural loading. Displacements were recorded using three LVDTs, one load cell, and one data logger. Two of the LVDTs were installed in the center of the upper and lower sides of the specimen to measure displacement, while one was also mounted perpendicular to the vertical sides of the beam to monitor any out-of-plane displacements. Loading was applied under displacement control using a hydraulic pump, while the applied load was measured using a load cell. Figure 4(b) presents a schematic view of the test setup.

3. Results and Discussion

The test results obtained were analyzed using both the observed failure modes (Figures 5–8) and the load-displacement curves derived for the specimens (Figures 9–11) with the effects of loading plate thickness, presence of openings, employed strengthening methods, and presence of grooves on load-bearing capacity and ductility as the most important parameters involved.

In the load-displacement curves, "Δ" and "P" stand for displacement in the upper surface and the applied load, respectively. The values of these parameters for maximum and ultimate loads are reported in Table 2, where "Pmax" and "Pu" denote the maximum and ultimate loads, respectively, and "Δco" and "Δcc" represent the corresponding displacements at the center of the top side. Moreover, "tp" is the thickness of the loading and support plates, while "f'_{co}" and "E_u" denote the compressive strength of the standard cylinder specimen of concrete and the energy absorbed by each beam specimen, respectively. The absorbed energy of each specimen is corresponding to the area under the load-displacement curve. It should also be noted that the ultimate failure point is equated with the point at which an abrupt decline occurs in load if this ever happens. Otherwise, 85% of the maximum load is taken as the ultimate load and the corresponding displacement is considered as the ultimate displacement [8, 24]. Given the fact that each specimen had its unique compressive strength, unified values of maximum load, and absorbed energy (i.e., $p_{\max,u}$ and $E_{u,u}$, respectively) were used in the relevant comparisons. The unified value of load-bearing capacity was obtained by converting the compressive strengths of all the specimens to the basic compressive strength of the mix design (i.e., 40 MPa) according to the following equation.

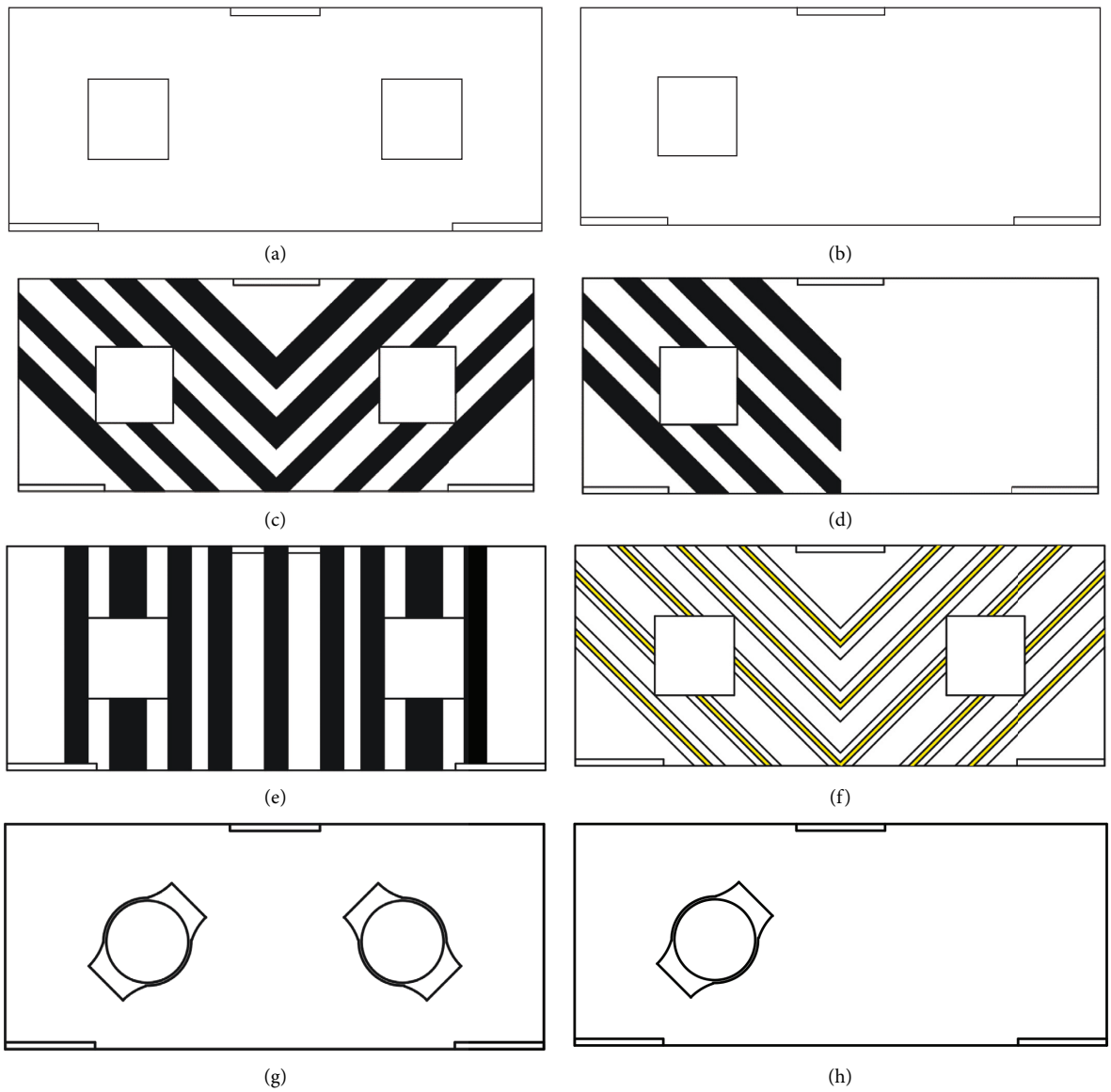

Figure 3: FRP-strengthening configuration in specimens: (a) specimen "*S*"; (b) specimen "*E*"; (c) specimens "S-EBR"; (d) specimen "E-EBR"; (e) specimen "*S-W*"; (f) grooves in specimen "S-EBROG"; (g) specimen "*S-F*"; and (h) specimen "*E-F*."

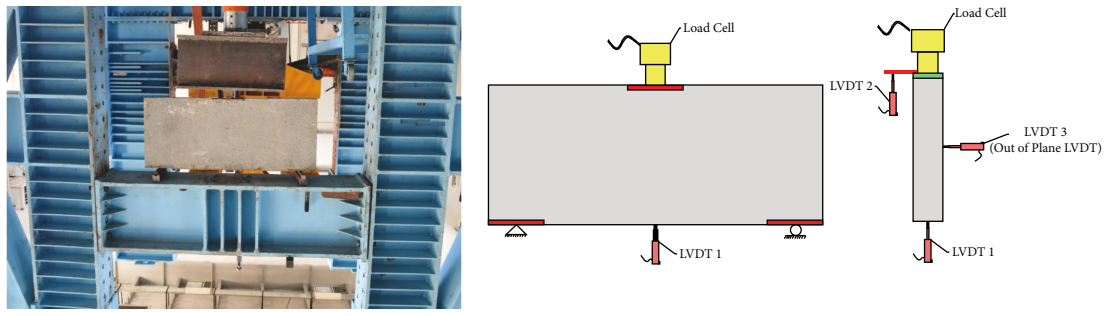

Figure 4: Test setup: (a) loading FRAME; (b) schematic representation of LVDTs and load cell installation (main and lateral sides).

(a) (b)

Figure 5: Failure modes of control specimens: (a) *C*1 and (b) *C*2.

Table 2: Test results.

Specimens	f'_{co}(MPa)	t_p (mm)	P_{max} (kN)	Δ_{co} (mm)	p_u (kN)	Δ_{cc} (mm)	E_u (N·m)	$P_{max,u}$ (kN)	$E_{u,u}$ (N·m)	$\frac{P_{max,u}}{P_{max\,0,u}}$	$\frac{E_{u,u}}{E_{u0,u}}$	$\frac{P_{max,u}}{P_{max,r,u}}$	$\frac{E_{u,u}}{E_{ur,u}}$
*C*1	42.1	30	565	7.84	480	9.68	3480	537	3309	1	1	1	1
*C*2	41.0	15	267	4.73	235	11.20	2341	230	2284	0.43	0.69	0.43	0.69
S	41.7	30	213	5.58	181	7.64	1104	204	1058	0.38	0.32	1	1
S-EBR	38.1	30	288	7.74	276	8.10	1375	302	1444	0.56	0.44	1.48	1.36
S-EBROG	42.0	30	310	9.13	264	10.67	2210	295	2103	0.55	0.64	1.45	1.99
S-W	40.7	30	289	7.44	246	10.86	2230	282	2195	0.53	0.66	1.38	2.07
S-F	44.7	30	473	14.49	473	14.49	5014	424	4487	0.79	1.36	2.08	4.24
E	40.9	30	187	4.56	159	5.68	656	182	641	0.34	0.19	1	1
E-EBR	37.0	30	250	7.48	213	8.33	1279	270	1382	0.50	0.42	1.48	2.16
E-EBROG	39.0	30	287	8.43	244	9.55	1805	294	1852	0.55	0.56	1.62	2.89
E-F	41.6	30	326	4.25	276	9.85	2542	314	2433	0.58	0.74	1.73	3.8

$$P_{max,u} = \sqrt{\frac{40}{f'_c}} * P_{max}. \quad (1)$$

By using (1), the last four columns in Table 2 report the ratios of maximum load carried by each specimen to those carried by the control ($P_{max,u}/P_{max,u,c}$) and the reference ($P_{max,u}/P_{max,u,r}$) specimens as well as the ratios of the energy absorbed by each specimen to those absorbed by the control ($E_u/E_{u,c,}$) and the reference ($E_u/E_{u,r}$) specimens. For reasons to be explained later, only the results obtained for the control specimen *C*1 were used for comparison in this study even though two kinds of control specimens (*C*1 and *C*2) had been constructed and tested. Moreover, the non-strengthened specimens "*S*" and "*E*" were used as reference specimens to compare the strengthening methods used for the specimens with symmetrically or asymmetrically positioned openings.

3.1. Failure Modes of the Specimens. Figures 5(a) and 5(b) depict the failure modes of *C*1 and *C*2. As already mentioned, these specimens only differed in their loading plate thickness. As reported in most previous studies experimenting with similar specimens [25–30], specimen *C*1 with a loading plate thickness of 30 mm exhibited diagonal cracks initiating from the inner edges of the supports that further extended to the loading plate. These cracks later grew in width as loading proceeded up to the failure point. Although the concrete around the loading plate in this specimen underwent a local failure, the failure mode was solely determined based on the diagonal cracks since concrete local failure was only observed under high levels of loading (next to the failure point) after diagonal cracks had already appeared and widened.

Diagonal cracks of low widths appeared in specimen *C*2 with a loading plate thickness of 15 mm, which gradually widened as loading proceeded and bending of the loading plate increased. The specimen ultimately failed after the loading plate had undergone enough bending, and the concrete experienced a complete local failure. As shown in Figure 5(b), this was accompanied by widespread cracking and fracturing of concrete in the areas around the loading plate. Therefore, it may be claimed that inadequate thickness of the loading plate caused the failure mode of this specimen to change from diagonal to local failure. Also, it may be mentioned that local failure is a premature failure in which the specimen fails to exploit its full strength.

In specimen "*S*" (Figure 6(a)), the first cracks formed about 35–40% of the maximum load. These cracks initiated from the corners of the opening toward the support point and later increased in number, while separate cracks also started to appear from each corner of the opening and propagated toward the loading and support points as loading proceeded. This observation confirms those reported in Kong [28]. It is observed in this figure that the cracks propagated symmetrically on both sides of the beam up to high loading levels (near the failure point) but that ultimate failure occurred when those on one side of the beam had already widened. The reason underlying the diagonal cracking pattern observed in all the specimens with openings is the tendency of the forces to transit from the loading to the support point over the shortest possible path; in beams without openings, the shortest path is a direct line between the support and the loading plates while the shortest path in

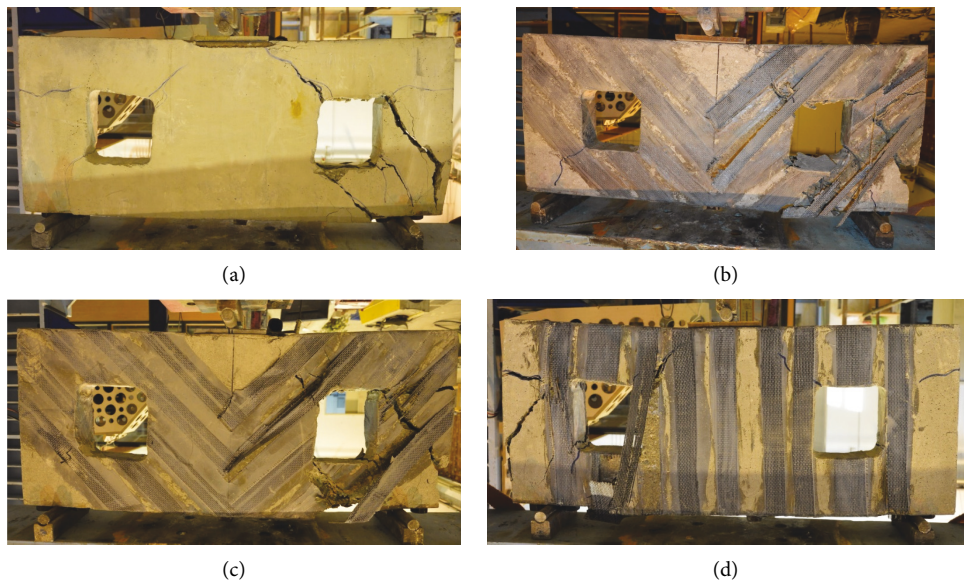

Figure 6: Failure modes of specimens with symmetrically positioned openings: (a) specimen *S*, (b) specimen S-EBR, (c) specimen S-EBROG, and (d) specimen *S-W*.

specimens with openings circumvents the openings. In addition to diagonal cracks as the main factor underlying specimen failure, flexural cracks appeared at about 50% of the maximum load in a region between the vertical side of the beam and the opening. These flexural cracks were created due to the short distance between the opening and the beam's vertical side that is under high flexural effects. Thus, the combination of flexural and diagonal cracks led to the much larger cracks in these specimens.

Although a cracking pattern similar to that in specimen "*S*" was observed on the side enclosing the opening in the specimen with asymmetrically positioned openings (i.e., specimen *E*), its other side with no openings exhibited much smaller cracks. This was attributed to the strength of the nonopening side that was much higher than that of the side with openings. The higher strength of the nonopening side also led to its lower contribution to the final failure of the beam (Figure 7(a)).

The specimens "S-EBR" and "E-EBR" exhibited a cracking behavior similar to that observed in the corresponding nonstrengthened specimens "*S*" and "*E*," respectively. The cracking pattern in these specimens propagated diagonally from one corner of the opening toward the support and loading points (Figures 6(b) and 7(b)). Moreover, observed FRP debonding indicated the insufficient shear strength formed between the FRP sheets and the substrate concrete. In addition to debonding, some of the FRP retrofits experienced rupture as a result of crossing wide cracks and exposure to high stresses. In other parts of these specimens, no spalling or rupture was observed despite the beam's cracking.

Up to high loading levels, the specimens "S-EBROG" and "E-EBROG" exhibited failure modes similar to those observed in other specimens with openings. However, much larger cracks appeared in the beams toward the end of the loading process due to the high impact of the FRP sheets as a result of the grooves, which ultimately caused big pieces of the substrate concrete to spall. Compared to the specimens lacking grooves, these specimens had more ruptured FRP sheets mostly on large cracks. However, most of the FRP sheets underwent a debonding failure accompanied by the spalling of big pieces of the substrate concrete. This failure mode may be attributed to the good shear strength created between the FRP retrofits and the substrate concrete due to the grooves (Figures 6(c) and 7(c)).

The cracking behavior in specimen "*S-W*" was similar to the other specimens. Cracks started from the corners of the openings and propagated toward the support and loading points, which transferred considerable amounts of the forces to the substrate concrete due to the confinement resulting from the FRP sheets wrapped around the specimens. This sequence of events finally caused great cracks to appear, and pieces of concrete to spall. Although some of the FRP sheets ruptured because of their location at the sharp edges of the beam section, no FRP debonding was observed in this specimen due to the adequate anchorage of FRP retrofits (Figure 6(d)).

There is a high tendency for trusses to form in specimen "*C-F*" due to the SPFs installed (Figure 8(a)). However, the heterogeneity of concrete and steel as well as the inadequacy of the shear strength between the frame and the concrete caused the SPF to detach from the concrete on one side, and the loads were diagonally transferred to the support point. It should be noted that forces are transmitted to the support points through SPF. It subsequently causes the width and the amounts of cracks to be decreased. If lateral stresses are ignored and only axial forces are taken into account, the SPF can then be viewed as a "two-force member" that transfers the forces axially without diverting their path. Given the spalling of the concrete surrounding

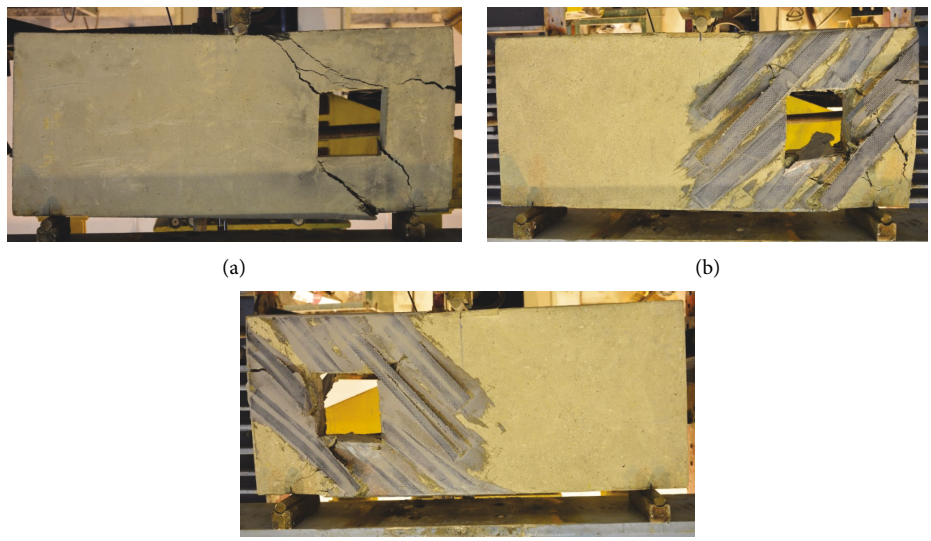

(a) (b)

(c)

Figure 7: Failure modes of specimens with asymmetrically positioned openings: (a) specimen *E*, (b) specimen E-EBR, and (c) specimen E-EBROG.

(a) (b)

Figure 8: Failure modes of specimens strengthened with SPFs: (a) specimen *S-F* and (b) specimen *E-F*.

the frame, it seems logical to hypothesize that lateral forces did not affect the frame. Nevertheless, mechanical joints around the frame can be used to ensure SPF–concrete continuity. In this situation, steel bars or mechanical ribs connected to the SPF can be used as joints that, when embedded sufficiently deep in concrete, will yield the desired connectivity between the frame and the concrete to prevent the detachment of the SPF from the concrete bulk. Despite the better truss performance of SPFs due to their being unaffected by lateral stresses, the technique is handicapped due to the frame-concrete discontinuity. The discontinuity between the frame and concrete has a decreasing effect on the structural performance of beams. This calls for further research to resolve this problem and to shed more light on the advantages and drawbacks of SPFs from a different perspective. In addition to the above, the high loads applied to the support and the stress concentration in concrete due to the presence of an SPF caused the concrete around the support point to spall, whereas the spalling had no notable effects on reducing final load-bearing capacity in the absence of large cracks.

Specimens "*E-F*" and "*C-F*" were similar not only in the behavior of their SPF retrofits but also in the debonding of their SPFs (Figure 8(b)). However, "*E-F*" exhibited differences in two essential respects; the first difference was the diagonal cracking in its side lacking openings, which is reasonably expected; and the second was its premature failure due to high-stress concentration in the concrete around the loading point. As shown in Figure 8(b), the concrete beneath the plate failed due to the bending of the loading plate, which led to the ultimate failure of the specimen. Even though this specimen does not provide much substance for predicting its loading capacity, the SPF's positive role in load transfer cannot be denied as judged from the cracking pattern around the SPF.

3.2. Effects of Loading Plate Thickness. Figure 9 presents the load-displacement curves for specimens "*C*1" and "*C*2." It is seen that the two curves are similar as far as their initial slopes are concerned. However, the loading plate in specimen "*C*2" bends due to its low thickness and that its displacement is larger than that of the control due to the bending. Hence, the term "Δ" in the curve begins to rise. The specimen reaches its maximum loading of 267 kN at a displacement of 4.73 mm, beyond which displacement rose

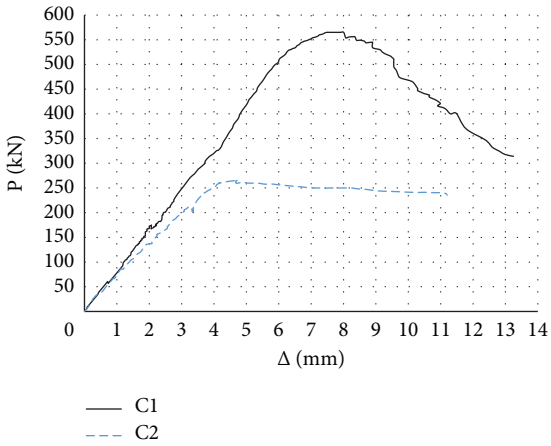

Figure 9: Load-displacement curves of the control specimens.

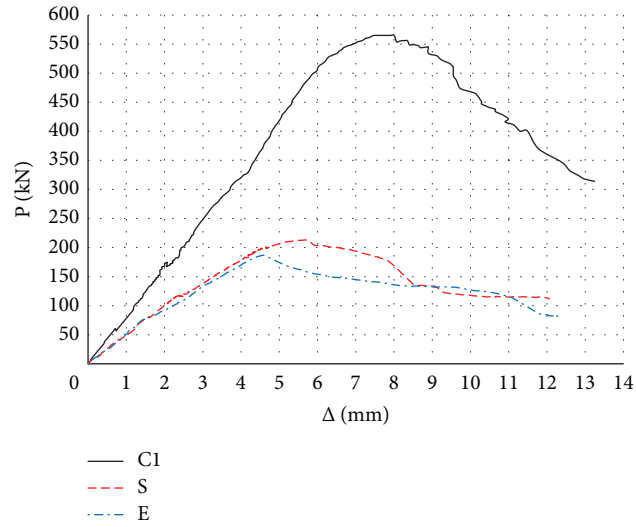

Figure 10: Load-displacement curves of the nonstrengthened specimens with openings.

with a constant slope of near-zero until a displacement of 11.20 mm as its ultimate loading was reached when the specimen failed. The near-zero slope observed in the second region of the curve for specimen "*C*2" indicates the predominant contribution of the loading plate behavior to the failure mode of the specimen. In contrast, the curve for specimen "*C*1" with an adequate plate thickness exhibits a slope steadily rising to its maximum loading of 565 kN for a corresponding displacement of 7.84 mm, which is higher than those of *C*2. Moreover, it is seen that the specimen exhibits a behavior characteristic of reinforced concrete structures in that it reaches its final state with its curve descending in a ductile manner after it reaches its maximum loading. Comparisons of the curves in Figure 8 and the displacement values reported in Table 2 reveal the greater displacement of "*C*2" than that of *C*1 since its behavior in the final loading stage is similar to that of steel. In terms of bearing capacity and energy absorption, however, *C*2 recorded values by 48% and 68%, respectively, lower than those of specimen "*C*1." The high decreases in these values indicate the important effects of loading plate thickness and, thereby, stress concentration on the load-bearing capacity of structural elements. Based on the above considerations and due to the premature failure of "*C*2," specimen "*C*1" was used as the control.

3.3. Effects of Opening. The load-displacement curves in Figure 10 derived for the three nonstrengthened specimens were used to investigate the effects of openings in deep beams. The first point to note in these curves is the differences among their initial slopes. The openings in these specimens intercept the stress transfer paths and, thereby, lead to drastic reductions in stiffness. Generally speaking, as a result of the high effects of stress transfer path dimensions on beam stiffness, any weak or defective zones in this path lead to the reduced overall stiffness of the member. Therefore, the presence of symmetrically or asymmetrically positioned square openings causes great decreases in beam stiffness. As shown in Figure 10, however, there is no linear relationship between the number of openings and the reduction in stiffness such that increasing the number of openings does not necessarily lead to further decreases in stiffness beyond a certain level. The reason for this might be sought in the instability of determinate trusses, in which instability is caused by decreasing degrees of freedom (to any level). In other words, the removal of only one member of the determinate truss suffices to make it unstable. Since the present deep beams are modeled as determinate trusses, removal of any number of members in them will have the same invariable effects. In other words, creating an opening and the resultant diversion in the stress transfer path can be interpreted as a kind of truss destabilization that is not affected by the number of openings made although the extent of instability of a beam with an opening in it is less than that of a beam without a strut. Thus, the destabilization effects can be used to determine the level of stiffness invariability. The higher the effects of an opening on the stress transfer path, the higher the effects of instability. Several factors are involved in beam instability, the most important of which are opening shape, dimensions, and position. For extremely low effects of opening on beam load capacity, beams will exhibit different behaviors depending on opening symmetricity. However, if the presence of an opening causes great reductions in beam load capacity, the effects of opening symmetricity will be negligible, and the beams with either symmetrically or asymmetrically positioned openings will exhibit the same behavior since the beam tends toward greater instability. This is partly verified by comparing the load-bearing capacities recorded for the two types of specimens. Defective or weak zones in stress transfer paths act as removed truss members that lead to reductions in the load-bearing capacity of the truss. Hence, the specimen with symmetrically positioned openings (S) reached its maximum load capacity of 213 kN at a displacement of 5.58 mm, representing a reduction of 62% in load capacity and 68% in energy absorption in comparison with the control specimen. The same values for the specimen with asymmetrically

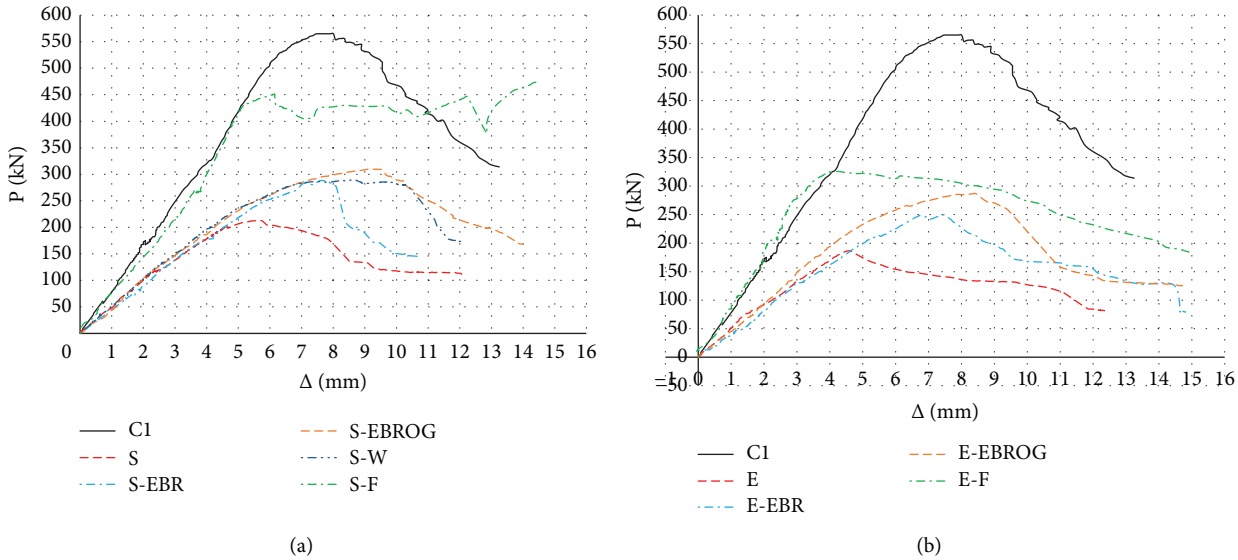

Figure 11: Load-displacement curves of the strengthened specimens: (a) specimens with symmetrically positioned openings and (b) specimens with asymmetrically positioned openings.

positioned openings were 187 kN and 4.56 mm, respectively, showing reductions of 67% and 81% relative to those of the control. Thus, it is observed that both kinds of symmetrically and asymmetrically positioned square openings in the stress transfer path caused notable decreases in load-bearing capacity, energy absorption, and stiffness with no significant differences between the two types of openings. Finally, the relevant curve shows that the ultimate load was reached with a gradually declining slope after the maximum load had been reached.

3.4. Effects of Strengthening Method. The diagrams in Figure 11 represent the behaviors of the specimens with either symmetrically or asymmetrically positioned openings. The strengthening methods used in these specimens include using CFRP composites with the EBR or EBROG techniques and using SPF.

3.4.1. The EBR Technique. The three specimens S-EBR, E-EBR, and *S-W* were retrofitted via the EBR technique. Figure 11 presents their load-displacement curves. It is observed that the curves of these three specimens exhibit initial slopes similar to those of the corresponding nonstrengthened ones. This is observed in all the specimens strengthened with FRP retrofits (via either the EBR or the EBROG technique). The identity of the initial slopes may be attributed to the way FRP sheets carry loads; for FRP sheets to be loaded in a specimen, at least one crack must have appeared in the concrete surface so that tensile stresses from the concrete would be transferred to the FRP retrofits. Since cracking in concrete appears beyond a certain load level, FRP retrofits do not come into play unless that certain load level is exceeded. In this way, the specimens might be viewed as nonstrengthened before this load level. Once the maximum load was reached, the three specimens reached their ultimate loads and failed in a ductile manner. From among the specimens strengthened via the EBR technique, "S-EBR" and "E-EBR" exhibited an increase of 42% and 41%, respectively, in their load-bearing capacities, while "*S-W*" showed an increase of 37% relative to those recorded by the reference ones (i.e., "*S*" and "*E*"). Moreover, the specimens "E-EBR," "*S-W*," and "S-EBR" recorded energy absorption increases of 105%, 104%, and 30%, respectively. Although these data indicate the less significant effect of the wrapping technique as compared to that of the inclined EBR, a comparison of the load-bearing capacities of these specimens with that of specimen "*C*1" reveals the higher energy absorption by "*S-W*." It must be noted that, compared to "*C*1," the specimens with an inclined configuration exhibited decreases of 58% to 61% in energy absorption, while the decrease recorded for "*S-W*" was only 35%. Regarding the fact that the failure mode in "*S-W*" was not accompanied by FRP debonding, it may be claimed that the wrapping technique yields energy absorption results superior to those achieved when the diagonal EBR technique is used. The reason for this might be the superior confinement of concrete in the wrapping technique. Although the wrapping technique was reasonably expected to lead to greater increases in load-bearing capacity, its effect on increasing energy absorption was decisive as well. Despite being insufficiently anchored, the inclined FRP retrofits used in the EBR technique were able to provide adequate load-bearing capacity in the specimen as a result of their orientation perpendicular to shear cracks. The reverse was true in the case of "*S-W*," in which adequate anchorage of the retrofits

to prevent their debonding led to a satisfactory load-bearing capacity in the specimen although the FRP retrofits were not oriented perpendicular to shear cracks.

Despite the many advantages of concrete confinement to improve the load capacity and ductility of beams, the large amount of FRP sheets needed and its inapplicability to slab-connected beams have led to a growing interest being nowadays shown to the inclined configuration in the EBR technique [8] as it has been found to improve concrete performance by preventing crack widening. It is, however, plagued with such disadvantages as lacking enough anchorage that causes the common problem of FRP debonding. The grooving technique has been recently proposed to overcome such problems.

3.4.2. The EBROG Technique. The two specimens "S-EBROG" and "E-EBROG" were used to investigate the effects of grooves used in the EBROG technique; the relevant load-displacement curves are presented in Figure 11. As already mentioned, FRP debonding is one of the principal failure modes, which takes place in the top side of ordinary beams (flexural strengthening) and the Web of deep beams (shear strengthening). The reason for debonding of FRP sheets in this technique is inadequate anchorage for them. The grooves made in the EBROG technique transfer more forces to the inner layers of concrete and, thereby, give rise to better adhesion of the retrofits to the substrate concrete. This, in turn, leads to an enhanced shear strength that delays the debonding event. Despite its widespread use in ordinary beams [18–20], application of the grooving technique in deep beams was only reported in Arabzadeh and Karimizadeh [8] who used grooves to strengthen deep beams with circular openings.

As was the case with the specimens strengthened via the EBR technique, the initial slopes of the load-displacement curves plotted for those strengthened through the EBROG technique are similar to those of the nonstrengthened specimens since the FRP retrofits have no effect on load-bearing capacity at low load levels. Generally speaking, the initial slope of the load-displacement curve is independent of the strengthening technique used. Effects of strengthening techniques become apparent once loading has reached 60% to 80% of the maximum load of the nonstrengthened specimen at which point the specimens undergo different failure modes depending on the strengthening technique employed.

It is seen in Figure 11 that specimen "S-EBROG" reached its maximum loading of 310 kN at a displacement of 9.13 mm beyond which ultimate load was achieved with a falling slope in a ductile manner as already observed with other specimens. According to Table 2, increasing load-bearing capacity in this technique was almost similar to those in specimens without grooves but energy absorption increased by about 60%. Moreover, this specimen recorded enhancements of 45% and 99% in load capacity and energy absorption, respectively, relative to those recorded for the reference specimen "*S*" but decreases of 45% and 36% relative to the values measured for the control specimen "*C*." Clearly, the grooving technique not only increases the energy absorbed but also has desirable effects on the failure mode of the specimen. As already described in the Section on failure modes above, not only is FRP debonding observed to occur in this specimen but FRP sheets are also seen to fracture and concrete pieces sticking to the FRP retrofits to spall; these serve as evidence supporting the efficacy of the technique. From a different perspective, although loading capacity did not vary in this specimen rather than the specimen without grooves, its greater energy absorption means the greater area under the curve and, thereby its improved ductility, which is important for structural design purposes. To gain a better understanding of the effects of the EBROG technique, the curve for "E-EBROG" is presented in Figure 11(b). According to this figure and Table 2, this specimen reached its maximum load of 287 kN at a displacement of 8.43 mm, beyond which it reached its ultimate load in a ductile manner as was the case with the other specimens. Thus, the grooves created in this specimen led to enhancements in load capacity and energy absorption. Compared to the EBR technique, the EBROG led to increases of 17% and 77% in load-bearing capacity and energy absorption, respectively. Compared to specimen "*E*" without any retrofits, "E-EBROG" experienced increases of 58% and 182% in its loading capacity and energy absorption, respectively, but decreases of 47% and 46% in the same parameters when compared with the "*C*1." In their previous study [8], the present authors observed that the cracking angle shifted toward a right angle as one of the effects of grooving in deep beams with circular openings, which was interpreted as increased loading capacity and ductility of the specimen. This cracking pattern is not observed in specimens with square openings since cracks in such cases tend to start from the corner of the openings. Indeed, FRP retrofits in deep beams function as shear strengthening means so that the shear capacity of the beam increases with increasing effect of FRP retrofits, thereby inducing a cracking pattern similar to that observed in ordinary beams (in which cracking is vertical). It is obvious that a flexural behavior in structural members is preferred to a shear one.

The use of the wrapping configuration is not feasible for strengthening deep beams not only due to on-site implementation problems but because of its associated high cost as well. Instead, the inclined configuration can be exploited for strengthening such beams to achieve appropriate load capacities by taking advantage of the high depth of such beams that offers a good opportunity for anchoring of retrofits. Alternatively, it might be claimed that the larger space deep beams provide for anchoring retrofits leads to the superior performance of the grooving technique in such beams rather than in ordinary ones. In sum, the high depth of the beam and the greater length of the FRP retrofit increase the effective anchorage length to delay early FRP debonding.

Based on these findings on specimens strengthened with FRP retrofits via the two EBR and EBROG techniques, and drawing upon the established effects of grooves on ordinary and deep beams with circular openings [8], the grooving technique may be recommended as a highly useful method for delaying or even preventing FRP debonding.

3.4.3. The SPF Technique. The load-displacement curves for specimens "*S-F*" and "*E-F*" are presented in Figures 11(a) and 11(b), respectively. It is observed that these curves exhibit initial slopes different from those of specimens strengthened with FRP retrofits. Two important notes may be mentioned for the differences observed. First, FRP retrofits, as already observed above, are activated to participate in load-bearing at loads equal to 70% to 80% maximum load. Hence, the initial slopes in the curves for the specimens thus strengthened are reasonably expected to correspond to those of the nonstrengthened ones. Unlike FRP retrofits, however, SPFs contribute to the load-bearing capacity from the very beginning of the loading process as a steel member is placed at the position of the opening; this naturally affects the initial slope of the curve. The second note is the stiffness of the specimens strengthened with SPFs is almost similar to that of the control specimen ("*C*1"). The replacement of a steel frame for the opening not only helps maintain the basic role of the opening to accommodate installations but also compensates for the low strength due to breakage of the strut. In other words, rather than transferring the loads through the medium of concrete, they are transferred directly through a steel frame that serves as a two-force member. Therefore, it is natural that far fewer declines are observed in such structural properties as stiffness and loading capacity. According to Figure 11(a) and Table 2, specimen "*S-F*" reached its maximum load of 473 kN at a displacement of 14.49 mm. This means a 19% decrease in loading capacity relative to that of specimen "*C*1" but a 115% increase relative to that measured for "*S*."

Experiencing a premature failure, specimen "*E-F*" reached its maximum load of 326 kN at a displacement of 4.25 mm, showing a reduction of 42% in load-bearing capacity when compared to "*C*1" but a 73% increase relative "*E*." Beyond the maximum load, the specimen "*S-F*" reached its ultimate load value, realized by a relatively horizontal line accompanied by great fluctuations in the curve. This behavior indicates the intense interlock of concrete and steel frame, the loss of which caused a sharp drop in loading capacity followed by rising segments before the next interlock. This process repeated itself several times before the ultimate load was finally reached. This behavior was not observed in "*E-F*" that exhibited behavior similar to that observed in strengthened specimens. That is, after reaching the maximum load, its curve declined in a ductile manner before it reached its ultimate load. These differences between the behaviors of "*E-F*" and "*S-F*" for load capacity and postpeak behavior could have been due to both premature failures of "*E-F*" and the positional symmetricity of their openings. Since steel frames are much stronger and stiffer than concrete, specimen "*S-F*" with two frames tends to exhibit a nonconcrete behavior. Rather than a falling curve characteristic of a concrete member, it has a horizontal curve that extends horizontally toward the ultimate load whereby the loading capacity also increases to a great extent. Specimen "*E-F*" exhibits a lower loading capacity. Although the frame in this specimen is expected to increase its capacity, the asymmetrically positioned openings caused the frame to play a less effective role when compared with the symmetrically positioned ones.

Specimen "*S-F*" absorbed more energy than "*C*1," as evidenced by the extension of its curve stretched beyond the maximum load point. The reason for this is the higher impact of two, rather than one, frames. Energy absorption was 337% higher in specimen "*S-F*" than "*S*." Similarly, specimen "*E-F*" absorbed 282% more energy than "*E*" although its energy absorption (considering its premature failure) was 27% less than "*C*1."

The conclusion to be drawn from the above observations is that load capacity in specimens could be increased even beyond that recorded by the control specimen (*C*1) only if proper connections are provisioned to interlock the frame and the concrete. Research endeavors in the future aimed at better exploitation of the steel frame advantages are recommended in quest of proper types of frame-concrete connections.

4. Conclusion

This study was devoted to the investigation of CFRP retrofits used to strengthen deep beams with square openings in them. The parameters examined included loading plate thickness, the strengthening technique (EBR or EBROG), opening positions (symmetrical or asymmetrical), and the use of steel protective frames. Eleven simply supported deep RC beams were subjected to the three-point monotonic loading test. While symmetrically or asymmetrically positioned square openings were created in some of the experimental beams and subsequently retrofitted with FRP composite sheets, openings with steel protective frames were made in others. Additionally, four nonretrofitted beams were used as either reference or control specimens for comparison of the test results. The most important findings of this experiment are as follows:

(i) The beams exhibited a shear failure and diagonal cracks that led to strut formation were generally observed in them. These cracks in the beams without openings typically started from the support plates and propagated toward the loading plate. In beams with either symmetrically or asymmetrically positioned openings, the cracks started either from the edges of the loading plate or the support plate and propagated toward the top or bottom corners of the openings, respectively, widening as loading proceeded before the specimen finally failed. Moreover, failure in all the specimens with asymmetrically positioned openings occurred in the zones hosting the openings while only small cracks of only slight effects on load capacity appeared in those that had no openings.

(ii) Inadequate thickness of the loading plate was observed to result in a local failure that is regarded to be a premature one.

(iii) Depending on the impact of openings on the ultimate load-bearing capacity of the beam, the

symmetricity of the opening positions was found to affect such structural properties as stiffness, loading capacity, and ductility such that the more these properties declined as a result of opening effects, the less significant were the effects of positional symmetricity of the openings and the beams would, therefore, tend to become unstable. In contrast, opening positional symmetricity was inversely related to opening effects on beam properties if these effects led to lower reductions in beam properties. In other words, deep beams with asymmetrically positioned openings exhibited higher load capacities than did those with symmetrically positioned openings. It was found that symmetrically positioned openings led to decreases of 62% and 68% in loading capacity and energy absorption, respectively, relative to those measured in the specimens without openings. The specimen with asymmetrically positioned openings recorded decreases of 67% and 81% for the same properties.

(iv) While the EBR technique led to the debonding of most FRP strips, the EBROG technique was observed to increase both loading capacity and energy absorption by changing the specimens' failure mode and by allowing the fracturing of some of the retrofitting strips rather than their debonding. The EBROG technique increased the shear strength and the effective length of the connection between the concrete and the retrofits by transferring the forces exerted on FRP sheets to the inner layers of concrete.

(v) The shear strength formed between the SPF and the concrete was observed to be lost at higher loads such that the SPF alone would ideally serve as a tow-force member to bear all the forces exerted on the strut. In real applications where the SPF might detach from the concrete to cause performance problems, mechanical joints (such as bars welded to the frame or ribs connected to it) might be used to secure their proper interlock; further investigation is needed to determine the properties and performance of such joints.

(vi) Specimens retrofitted via the EBR technique exhibited a superior performance as their loading capacity and energy absorption were enhanced by 42% and 105%, respectively, relative to those of the reference beam. This is while these same values for the specimens retrofitted via the EBROG technique were 58% and 182%, respectively, and 115% and 337% for those strengthened with SPFs.

Data Availability

No data were used to support this study.

Conflicts of Interest

The authors declare that they have no conflicts of interest.

References

[1] C. C. Tseng, S. J. Hwang, and W. Y. Lu, "Shear strength prediction of reinforced concrete deep beams with web openings," *ACI Structural Journal*, vol. 114, no. 6, pp. 1569–1579, 2017.

[2] I. Chengeni and A. Dalvand, "Finite element study of reinforced concrete deep beams with rectangular web openings," *Journal of Engineering and Applied Sciences*, vol. 11, no. 14, pp. 3167–3176, 2016.

[3] T.-M. Yoo, J.-H. Doh, H. Guan, and S. Fragomeni, "Experimental behaviour of high-strength concrete deep beams with web openings," *The Structural Design of Tall and Special Buildings*, vol. 22, no. 8, pp. 655–676, 2013.

[4] K. Senthil, A. Gupta, and S. Singh, "Computation of stress-deformation of deep beam with openings using finite element method," *Adv Concr Constr*, vol. 6, pp. 245–268, 2018.

[5] G. Campione and G. Minafò, "Behaviour of concrete deep beams with openings and low shear span-to-depth ratio," *Engineering Structures*, vol. 41, pp. 294–306, 2012.

[6] H. Karimizadeh and A. Arabzadeh, "A STM-based analytical model for predicting load capacity of deep RC beams with openings," *Structures*, vol. 34, pp. 1185–1200, 2021.

[7] T. El Maaddawy and S. Sherif, "FRP composites for shear strengthening of reinforced concrete deep beams with openings," *Composite Structures*, vol. 89, no. 1, pp. 60–69, 2009.

[8] A. Arabzadeh and H. Karimizadeh, "Experimental study of RC deep beams with opening and FRP composites installed by means of EBR and EBROG methods," *Construction and Building Materials*, vol. 208, pp. 780–791, 2019.

[9] S. Thuc Ha, *Design of concrete Deep Beams with Openings and Carbon Fiber Laminate Repair*, San Jose State University, San Jose, California, 2002.

[10] T. El-Maaddawy and B. El-Ariss, "Behavior of concrete beams with short shear span and web opening strengthened in shear with CFRP composites," *Journal of Composites for Construction*, vol. 16, no. 1, pp. 47–59, 2012.

[11] A. Bilotta, C. Faella, E. Martinelli, and E. Nigro, "Design by testing procedure for intermediate debonding in EBR FRP strengthened RC beams," *Engineering Structures*, vol. 46, pp. 147–154, 2013.

[12] G. Sas, C. Dăescu, C. Popescu, and T. Nagy-György, "Numerical optimization of strengthening disturbed regions of dapped-end beams using NSM and EBR CFRP," *Composites Part B: Engineering*, vol. 67, pp. 381–390, 2014.

[13] M. A. Hosen, M. Z. Jumaat, U. J. Alengaram, N. R. Sulong, and A. S. Islam, "Structural performance of lightweight concrete beams strengthened with side-externally bonded reinforcement (S-EBR) technique using CFRP fabrics," *Composites Part B: Engineering*, vol. 176, Article ID 107323, 2019.

[14] A. Hajihashemi, D. Mostofinejad, and M. Azhari, "Investigation of RC beams strengthened with prestressed NSM CFRP laminates," *Journal of Composites for Construction*, vol. 15, no. 6, pp. 887–895, 2011, –895.

[15] A. Bilotta, F. Ceroni, E. Nigro, and M. Pecce, "Efficiency of CFRP NSM strips and EBR plates for flexural strengthening of RC beams and loading pattern influence," *Composite Structures*, vol. 124, pp. 163–175, 2015.

[16] S. J. E. Dias, J. A. O. Barros, and W. Janwaen, "Behavior of RC beams flexurally strengthened with NSM CFRP laminates," *Composite Structures*, vol. 201, pp. 363–376, 2018.

[17] M. A. Hosen, M. Z. Jumaat, A. S. Islam, M. Kamruzzaman, M. N. Huda, and M. R. Soeb, "Eliminating concrete cover

separation of NSM strengthened beams by CFRP end anchorage," *Structural Engineering & Mechanics*, vol. 56, no. 6, pp. 899–916, 2015.

[18] D. Mostofinejad and S. M. Shameli, "Externally bonded reinforcement in grooves (EBRIG) technique to postpone debonding of FRP sheets in strengthened concrete beams," *Construction and Building Materials*, vol. 38, pp. 751–758, 2013.

[19] D. Mostofinejad and A. Tabatabaei Kashani, "Experimental study on effect of EBR and EBROG methods on debonding of FRP sheets used for shear strengthening of RC beams," *Composites Part B: Engineering*, vol. 45, no. 1, pp. 1704–1713, 2013.

[20] D. Mostofinejad and A. Moghaddas, "Bond efficiency of EBR and EBROG methods in different flexural failure mechanisms of FRP strengthened RC beams," *Construction and Building Materials*, vol. 54, pp. 605–614, 2014.

[21] D. Mostofinejad and E. Mahmoudabadi, "Grooving as alternative method of surface preparation to postpone debonding of FRP laminates in concrete beams," *Journal of Composites for Construction*, vol. 14, no. 6, pp. 804–811, 2010.

[22] D. Mostofinejad and M. J. Hajrasouliha, "Experimental study on grooving detail for elimination of debonding of FRP sheets from concrete surface," in *Proceedings of the 5th International Conference on FRP Composites in Civil Engineering (CICE 2010)*, Beijing, China, September 2010.

[23] Aci Committee 318, *Building Code Requirements for Structural Concrete (ACI 318-14) Commentary on Building Code Requirements for Structural Concrete (ACI 318R-14) an ACI Standard and Report*, American Concrete Institute, Farmington Hills, MI, 2014.

[24] H. Karimizadeh, M. R. Eftekhar, and D. Mostofinejad, "Effects of midlayer used in FRP confinement of RC columns," *Journal of Composites for Construction*, vol. 23, no. 2, Article ID 04019002, 2019.

[25] H. A. R. de Paiva, *Strength and Behavior in Shear of Deep Reinforced Concrete Beams Under Static and Dynamic Loading*, University of Illinois, Urbana Champaign,Illinois, 1961.

[26] V. Ramakrishnan and Y. Ananthanarayana, "Ultimate strength of deep beams in shear," *Journla. Proceedings*, vol. 65, pp. 87–98, 1968.

[27] F. K. Kong, R. C. Garcia, J. M. Paine, C. W. J. Tang, and M. Chemrouk, "Strength and stability of slender concrete deep beams," *Structural Engineer*, vol. 64, pp. 49–56, 1986.

[28] F. K. Kong, *Reinforced Concrete Deep Beams*, CRC Press, Boca Raton, Florida, 1991.

[29] K. H. Tan, C. Y. Tang, and K. Tong, "A direct method for deep beams with web reinforcement," *Magazine of Concrete Research*, vol. 55, no. 1, pp. 53–63, 2003.

[30] K. S. Ismail, M. Guadagnini, and K. Pilakoutas, "Strut-and-Tie modeling of reinforced concrete deep beams," *Journal of Structural Engineering*, vol. 144, no. 2, Article ID 04017216, 2018.